

Thermodynamic compensation to temperature extremes in *B. subtilis* vs *T. maritima* lysine riboswitches

Andrea Marton Menendez^{1,2,*} and David J. Nesbitt^{1,2,3,*}

¹JILA, University of Colorado Boulder and National Institute of Standards and Technology, Boulder, Colorado; ²Department of Chemistry, University of Colorado Boulder, Boulder, Colorado; and ³Department of Physics, University of Colorado Boulder, Boulder, Colorado

ABSTRACT *T. maritima* and *B. subtilis* are bacteria that inhabit significantly different thermal environments, ~80 vs. ~40°C, yet employ similar lysine riboswitches to aid in the transcriptional regulation of the genes involved in the synthesis and transport of amino acids. Despite notable differences in G-C basepair frequency and primary sequence, the aptamer moieties of each riboswitch have striking similarities in tertiary structure, with several conserved motifs and long-range interactions. To explore genetic adaptation in extreme thermal environments, we compare the kinetic and thermodynamic behaviors in *T. maritima* and *B. subtilis* lysine riboswitches via single-molecule fluorescence resonance energy transfer analysis. Kinetic studies reveal that riboswitch folding rates increase with lysine concentration while the unfolding rates are independent of lysine. This indicates that both riboswitches bind lysine through an induced-fit (“bind-then-fold”) mechanism, with lysine binding necessarily preceding conformational changes. Temperature-dependent van’t Hoff studies reveal qualitative similarities in the thermodynamic landscapes for both riboswitches in which progression from the open, lysine-unbound state to both transition states (\ddagger) and closed, lysine-bound conformations is enthalpically favored yet entropically penalized, with comparisons of enthalpic and entropic contributions extrapolated to a common $[K^+] = 100$ mM in quantitative agreement. Finally, temperature-dependent Eyring analysis reveals the TMA and BSU riboswitches to have remarkably similar folding/unfolding rate constants when extrapolated to their respective (40 and 80°C) environmental temperatures. Such behavior suggests a shared strategy for ligand binding and aptamer conformational change in the two riboswitches, based on thermodynamic adaptations in number of G-C basepairs and/or modifications in tertiary structure that stabilize the ligand-unbound conformation to achieve biocompetence under both hyperthermophilic and mesothermophilic conditions.

SIGNIFICANCE Microbes in extreme environments develop a variety of strategies to survive. Among them, their RNA can acquire additional tertiary structure, G-C basepairing, or ligand binding to stabilize important features at higher temperatures. Riboswitches are portions of RNA that bind a ligand to stabilize open and closed conformations to facilitate or block gene expression. Lysine riboswitch aptamers in *B. subtilis* versus *T. maritima* have similar secondary and tertiary structures despite operating at 40 vs. 80°C. We study lysine- and temperature-dependent binding and folding kinetics of each via single-molecule FRET microscopy. The results indicate that evolution in G-C basepairing and tertiary interactions tune the *T. maritima* and *B. subtilis* aptamer conformational stability to bind lysine and fold biocompetently despite significant differences in environmental temperature.

INTRODUCTION

Microorganisms are found in nearly all natural environments, inhabiting climate conditions at extremes of temperature, pH, salinity, or pressure, which necessitate a variety of adaptations to survive (1–4). Cells can adjust their mem-

brane lipid composition or proton permeability to account for rigidity changes in very hot/cold or high-pressure conditions, or to maintain appropriate intracellular pH in highly basic or acidic environments (1,5). Heat and cold shock proteins may be generated that can act as chaperones to maintain proper synthesis, conformation, and biochemical activity of other proteins to protect the cell from temperature extremes (6). In addition, microbes have evolved several RNA-based mechanisms to accommodate their specific conditions such as RNA thermometers (7–8), segments of RNA

Submitted March 12, 2024, and accepted for publication July 29, 2024.

*Correspondence: andrea.marton@colorado.edu or djn@jila.colorado.edu

Editor: Susan Schroeder.

<https://doi.org/10.1016/j.bpj.2024.07.039>

© 2024 Published by Elsevier Inc. on behalf of Biophysical Society.



that control protein synthesis by melting at higher temperatures to expose a ribosome binding site, and riboswitches (9–11), which bind a target ligand to change conformational state to allow or block transcription, translation, or splicing based on in situ concentration of specific metabolites. At an even more basic level, adaptations in RNA that create additional structural features can accumulate to protect RNA from heat: increased G-C basepairing in stem regions, small ligand binding, and additional tertiary interactions such as hydrogen bonds, cross-strand or intrastrand stacking interactions, or water/metal bridges can all serve to shield RNA from heat denaturation to preserve functionality (12–13). Cooperatively paired adaptations are common due to the prevalence of environments with multiple extreme conditions, such as high temperatures and pressures in deep-sea thermal vents or variable pH/temperature conditions as in acidic/alkaline hydrothermal springs (3,14). Survival strategies for extremophilic microorganisms under such harsh conditions highlight underlying evolutionary advantages, offering insights into mechanisms for extraterrestrial life (15–16) and as potential sources of enzymes for efficient and “green” industrial processes (17–19).

Many bacteria (20–21), archaea (22–23), and eukaryotes (24) across a wide variety of environments make use of riboswitches encoded within the mRNA as efficient regulators of gene expression (25–28). Riboswitches are segments of noncoding RNA consisting of an aptamer and expression platform, usually found in the 5′ untranslated mRNA region directly upstream of the gene they control. The aptamer portion of a riboswitch can adopt at least two conformations generally categorized as “open” or “closed” states and contains a binding pocket that selectively binds to a ligand (27,29), a small molecule (30–31), or ion (32), often with 10- to 1000-fold preference for the target versus closely related metabolite species (33–36). The aptamer undergoes many crucial and often subtle conformational changes between open or closed states, which are facilitated or stabilized by ligand binding. This results in significant secondary or tertiary structural changes to the adjacent expression platform, which in turn switches between “on” and “off” states whereby gene expression can proceed or be terminated (37–38). Families of riboswitches have been identified whose aptamers respond to a plethora of ligands such as purines (30,39), amino acids (31,40), metal cations (41–42), and metabolites (43), with riboswitches even synthetically developed to bind to specific molecules relevant to biosensing (44–45) or antimicrobial drug development (46). Consequently, the mechanisms by which aptamers identify and bind to ligands are critically important in gene regulation for many organisms and provide key functionality advantages for responding to changes in the intracellular environment. Two limiting kinetic scenarios for riboswitch folding are often described in terms of the relative order for ligand binding and RNA conformational change, induced-fit (IF) and conformational selection,

although the process often occurs as a combination of the two. In the IF (“bind-then-fold”) mechanism, binding of a target ligand necessarily precedes and triggers folding from the open to closed state in the riboswitch. Conversely, in the conformational selection (CS) pathway (“fold-then-bind”), the riboswitch interconverts transiently between open and closed states, with free energies for the closed conformation preferentially stabilized by subsequent binding of the ligand (47).

Lysine riboswitches exist in numerous bacterial phyla, representing mesophilic bacteria from Fusobacteriota, Bacillota (in which *B. subtilis* [BSU] is found), and Gammaproteobacteria, among others, as well as those that inhabit extreme temperature or acidic conditions as in Thermotoga (home to *T. maritima* [TMA]) and Acidobacteriota (43). Lysine riboswitches can regulate transcription or translation of genes in dramatically different environments yet often share several key motifs and have highly conserved secondary and tertiary structures in their aptamer moieties. In one such example, the BSU and TMA lysine riboswitch aptamers (see Fig. 1) share several important tertiary structures (34,48,49), but BSU is typically found in soils and animal digestive tracts (50) at around 40°C while TMA was first identified near thermal vents on the seafloor and has an optimal growth temperature of 80°C (51). The main focus of this work is exploring temperature-dependent similarities/differences in riboswitch ligand binding strategies via single-molecule TIRF microscopy, to better characterize how BSU and TMA may have evolutionarily adapted to their different thermal environments.

Despite similar tertiary structures, the BSU (40) and TMA (34) riboswitch aptamers (see Fig. 1) exhibit significant differences in their primary sequences. In particular, there are more G or C bases (GC content) in TMA (66%) over BSU (44%) riboswitches, which translates into a significantly higher percentage of G-C basepairs in TMA (76%) vs. BSU (44%). These G-C pairs (Fig. 1, highlighted in red) contribute significantly to thermodynamic stability of the corresponding riboswitch secondary structures, with the GC content in RNA shown to correlate positively with optimal growth temperatures in many prokaryotes (52–54). By way of contrast, the larger tertiary structure motifs in the two riboswitch aptamers are quite similar despite such differences in primary structure: both are comprised of five helices that come together to create a five-way junction that binds the cognate ligand and features an interaction between the internal loop in P2 and the terminal loop in P4 as well as an important P2-P3 kissing loop interaction, as depicted in Fig. 1, a and b (55). In addition, transcriptional control in both riboswitches is based on the expression platform creating terminator or antiterminator stems that prevent or allow P1 to be fully formed, which is in turn stabilized by the presence of lysine (40,48,49). These tertiary structures are thought to be formed cotranscriptionally and are required for the riboswitches to bind lysine and fold

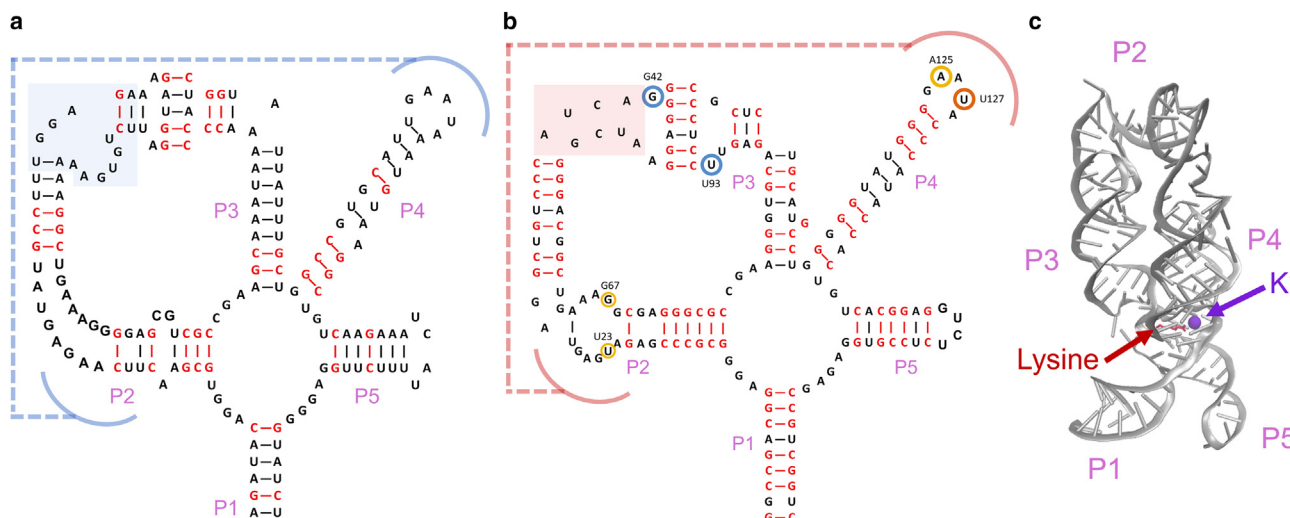


FIGURE 1 *B. subtilis* (BSU) and *T. maritima* (TMA) lysine riboswitch aptamers with P1 fully formed: (a) BSU and (b) TMA basepairing with G-C basepairs highlighted in red. Both aptamers exhibit a five-way helical junction and long-range “kissing loop” interactions between P2 and P3, although there is significantly more G-C pairing in TMA (76%) than BSU (44%), residues involved in important tertiary interactions circled in blue, orange, or yellow, arched lines indicate interacting segments of the riboswitches. The kink-turn (BSU) and internal loop (TMA) motifs that enable the P2-P3 interaction are highlighted in blue and red, respectively. (c) Crystal structure of the TMA aptamer bound to lysine and K⁺ (PDB: 3DIL).

properly (56). In addition, previous studies into the kinetics and thermodynamics of the BSU riboswitch have shown the folding rate (k_{fold}) to be strongly dependent on [Lys], while the unfolding rate (k_{unfold}) remains independent of lysine concentration (56,57). This is clear evidence for an IF folding mechanism, in which lysine binding to the open state (O) is a prerequisite to aptamer conformational change into the closed state (C) and thus facilitates successful gene regulation. Furthermore, temperature-dependent kinetics reveal overall folding (O \rightarrow C) to be strongly exothermic ($\Delta H^\circ = -24$ kcal/mol) with substantial entropic barriers ($T\Delta S^\ddagger = -20$ kcal/mol at 300 K) to the transition state (57). Interestingly, although the majority of enthalpy release occurs *after* the folding transition state ($-\Delta H^\circ \rightarrow^\ddagger < -\Delta H^\ddagger \rightarrow^C$), most of the compensating entropic penalty (presumably due to greater organization of the riboswitch/lysine) takes place *before* the folding transition state ($-T\Delta S^\circ \rightarrow^\ddagger > -T\Delta S^\ddagger \rightarrow^C$). This would be consistent with a transition state with relatively few stabilizing hydrogen bonds, base stacking, and other interactions formed between lysine and RNA and within the RNA, but for which the riboswitch has largely completed any conformational change. Mechanistically, this suggests that only a few hydrogen bonds are required to modulate folding and thereby turn transcription on/off.

The above observations immediately imply a simple but important corollary. If BSU takes advantage of exothermic bond formation to overcome entropic penalties to folding, then by simple thermodynamic considerations such a strategy should be less effective at promoting lysine binding and folding under higher-temperature conditions. This would suggest that TMA might require a significantly different folding mechanism (e.g., enthalpically penalized

($\Delta H^\circ \gg 0$) with favorable entropic contributions ($T\Delta S^\circ \gg 0$)), or otherwise compensate for a decreased folding efficiency at higher temperatures. The central theme of this work focuses on temperature-dependent single-molecule total internal reflection microscopy (smTIRF) on BSU and TMA lysine riboswitches to further elucidate this simple but fundamental question.

The organization of this manuscript is as follows. We first present results on BSU and TMA folding kinetics with respect to lysine concentration via smTIRF to infer that the two riboswitches share a bind-then-fold (IF) pathway that requires lysine binding to precede conformational changes. Next, we present temperature-dependent kinetic data to create energy landscapes that surprisingly reveal folding to be a strongly enthalpically favored and entropically costly process in *both* BSU and TMA riboswitches. However, at the same temperature and [Na⁺], [Mg²⁺], [Lys], and [K⁺], BSU and TMA folding and unfolding dynamics occur on disparate timescales which prevents the collection of such kinetic data under identical ionic salt conditions. Indeed, at room temperature ($\sim 22^\circ\text{C}$) and physiologically relevant conditions ([Na⁺] = 100 mM, [Mg²⁺] = 0.5 mM (58), and [Lys] = 2 mM (59)), the two riboswitches require quite different [K⁺] ranges (1–20 mM for TMA and 100–200 mM for BSU) for folding/unfolding to occur on the same experimentally accessible timescales. Specifically, the TMA riboswitch folding rate at 20–100 mM [K⁺] is so fast ($t_{\text{fold}} \ll 0.1$ s) and the unfolding rate so slow ($t_{\text{unfold}} \gg 10$ s) that very few unfolding events occur before Cy3/Cy5 pair photobleaching, with the reverse scenario true for the BSU riboswitch. As a result, we explore and report enthalpic, entropic, and free energy contributions for TMA over a series of potassium

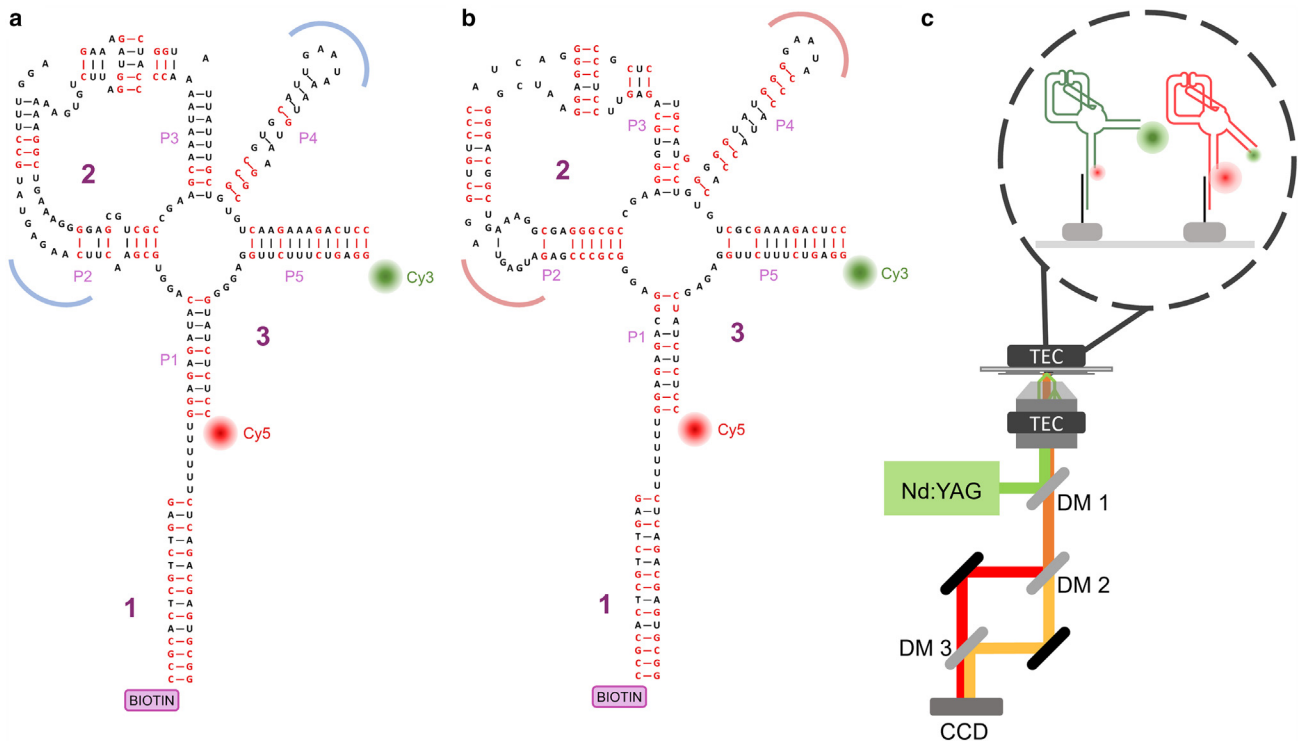


FIGURE 2 (a) BSU and (b) TMA aptamers used in experiments adapted from riboswitch aptamers (see Fig. 1 *a* and *b*) into three-stranded constructs, each with a biotinylated tethering strand, a main RNA strand beginning with extended and modified P1 and P5 segments, and a Cy3-Cy5 doubly labeled strand. (c) smTIRF instrument: an Nd:YAG laser is directed through a high N.A. objective, offset from the optical axis such that the beam hits the sample surface at the appropriate TIR angle. Fluorescent emission from the Cy3/Cy5 is collected through the objective, separated into donor (yellow) and acceptor (red) channels, and imaged onto a CCD camera.

concentrations (at constant $[\text{Na}^+] = 100 \text{ mM}$, $[\text{Mg}^{2+}] = 0.5 \text{ mM}$, and $[\text{Lys}] = 2 \text{ mM}$) with which to extrapolate to $[\text{K}^+] = 100 \text{ mM}$ conditions and enable direct comparison between TMA and BSU folding kinetics. We find enthalpic and entropic contributions between the open, transition, and closed states for the two riboswitches extrapolated to the same $[\text{K}^+]$ to be in surprisingly quantitative agreement. We therefore propose that differences in G-C basepairing or small but significant differences in tertiary structure between riboswitch sequences successfully tune TMA and BSU riboswitch stabilities to match at their respective 80 and 40°C thermal environments, such that folding/unfolding kinetics can maintain efficiency despite the diversity in ambient temperature conditions.

MATERIALS AND METHODS

We investigate the lysine concentration and temperature-dependent kinetics of riboswitch conformational changes via single-molecule fluorescence resonance energy transfer (smFRET) TIRF microscopy (60). To perform these studies, we modify the riboswitch aptamers into three-stranded RNA constructs as depicted in Fig. 2, *a* and *b*: 1) a biotinylated tethering strand basepairs with 2) the lengthened 5' end of P1 moiety of the main RNA strand, whose P5 helix is separated and lengthened to basepair with 3) a doubly labeled RNA strand with Cy3/Cy5 bound to the distal ends of the P1/P5 segments. These modifications have several important impli-

cations. First, extending the P1 and P5 sections of the aptamers from 7 bp in the wild-type P5 sections to 13/11 bp in the BSU/TMA constructs and from 6/8 bp in the BSU/TMA wild-type P1 sections to 10/8 bp in the BSU/TMA constructs dramatically stabilizes the constructs compared with the wild-type aptamers. In fact, each additional basepair decreases the amount of time necessary for duplexing (increases k_{on}) by about 0.8–0.6 \times and increases the amount of time the duplex stays together (decreases k_{off}) by about 10 \times (61). This means that once annealed, the reporter strand is very unlikely to unbind from the P1/P5 sections, which effectively results in “prefolded” aptamers. This means that lysine binding to the RNA may be faster, as the binding pocket is more intact than it would be in the wild-type aptamers.

The assembly efficiency of such a FRET construct (Fig. 2, *a* and *b*) is verified in multiple ways. First of all, HPLC is used to purify the fully assembled (three-strand) construct, with 10–20% excess of both [tethering strand] > [labeling strand] > [riboswitch strand] to saturate the riboswitch sequence, which is transcribed from the DNA template and then gel purified (56,62,63). The data from the HPLC purification results indicate annealing efficiencies >70% as a lower limit, with corresponding efficiencies for other three-strand FRET constructs found to be >90% as confirmed by both HPLC and PAGE methods (62–65). Secondly, we have capability in a separate confocal apparatus for two-color (green/red laser) alternating laser excitation (66), which allows us to confirm that constructs tethered to the surface contain both fluorophores, thereby ruling out damage to the covalent fluorophore linkage. Furthermore, we have also annealed under reverse-order concentration conditions, with [labeling strand] > [riboswitch strand] > [tethering strand], for which we can be confident that each surface immobilized construct contains all three components. The results from these studies are all consistent with >70% as a reliably conservative estimate of assembly efficiency. Most importantly, the

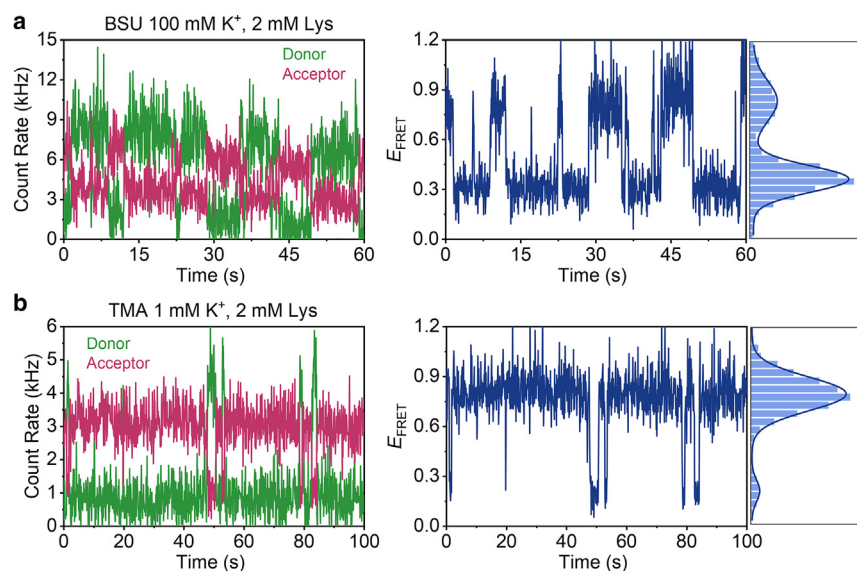


FIGURE 3 Sample data collected from the (a) BSU and (b) TMA riboswitch aptamers. Cy3 (green, donor) and Cy5 (pink, acceptor) intensities (left panels) are recorded and converted into FRET efficiency time traces (right panels), which switch between two discrete high (~ 0.8) and low (~ 0.3) FRET states. Both samples contain 100 mM Na^+ and 0.5 mM Mg^{2+} and were collected at 23°C.

labeling strand can only hybridize with the riboswitch strand and does not anneal directly to the tethering strand. Thus, FRET data for immobilized species tethered to the cover slip surface offer a further layer of preselection for the complete three-strand construct.

In the TIRF experimental apparatus (see Fig. 2 c), a 532 nm beam from a solid-state Nd:YAG (MeshTel GSF32–300PS) laser is sent through the back aperture of the microscope objective (Olympus PLAPON60XOSC2, Tokyo, Japan) with parallel lateral displacement from the optical axis. (The reporting of specific product names is for clarity purposes only and does not represent a statement of support by NIST.) This displacement tunes the angle of incidence of the beam onto the sample to generate total internal reflectance conditions and thereby simultaneously illuminate multiple Cy3-Cy5-labeled RNA molecules in the evanescent near field. Fluorescent emission from the Cy3 and Cy5 is then collected through the same objective, separated by a 645 nm LP dichroic mirror (Chroma DRLP) into donor and acceptor channels, recombined via a second dichroic mirror and imaged onto a CCD camera (Princeton Instruments I-PentaMAX 512-EFT, Trenton, NJ, USA). A small lateral offset between Cy3 and Cy5 fluorescence paths allows images to be recorded separately into donor/acceptor channels, with Cy3/Cy5 intensity ratios from colocalized molecules in the two channels used to obtain time-dependent FRET trajectories simultaneously from ~ 100 RNA molecules. The high-throughput advantage of TIRF detection is crucially important since unfolding kinetics for the TMA riboswitch under biologically relevant salt conditions at room temperature is quite slow ($\sim 0.1 \text{ s}^{-1}$) and therefore constrained by photobleaching rates (Fig. 3).

Samples are prepared in sandwich-style glass chambers as described previously (63,65,67), with a glass coverslip attached to the glass slide by two strips of double-sided sticky tape separated by a $\sim 2 \text{ mm} \times 10 \text{ mm} \times 300 \mu\text{m}$ flow channel. Four solutions are sequentially introduced through the channel to 1) passivate the glass slide with bovine serum albumin (10% biotinylated), 2) create streptavidin tethering sites on the passivated surface, 3) tether biotinylated RNA molecules, and 4) introduce a buffer solution (50 mM HEPES) with appropriate salts (100 mM NaCl, 0.5 mM MgCl_2 , and requisite KCl and lysine) and an oxygen-scavenging system (Trolox/PCA/PCD) to inhibit Cy3/Cy5 photobleaching. Each solution incubates for 10 min before the next solution is flushed through the channel; once the buffer solution is introduced, the sample channels are sealed with epoxy at each end to prevent evaporation during data collection.

Temperature control is achieved via a pair of thermoelectric coolers (TEC, TE Technology HP-127-1.0-0.8, Traverse City, MI, USA) clamped around the microscope objective and placed on top of the sample, providing $\pm 0.05^\circ\text{C}$ stability with which to perform temperature-dependent kinetic studies. Ideally, riboswitch folding kinetics for BSU and TMA would be measured at their respective environmental temperatures, 40 or 80°C. However, to take advantage of the high-throughput data collection afforded by TIRF microscopy, we are limited to heating the entire sample surface to $<40^\circ\text{C}$ to avoid damage to the microscope objective by softening of the optical cement. For quantitative comparison, we assume ΔH^\ddagger and ΔS^\ddagger to be temperature independent over the measured range (20–40°C) and calculate ΔG° and ΔG^\ddagger for the relevant riboswitch environmental conditions (40 or 80°C). All data reported typically reflect ~ 300 folding/unfolding events from 20 to 30 different RNA constructs to ensure adequate statistical sampling and signal to noise ratios.

To determine single-molecule folding and unfolding rate constants, we analyze time-dependent fluorescence intensity data from colocalized donor/acceptor FRET pairs. All time traces show characteristic anticorrelated behavior between Cy3 and Cy5 fluorescence episodes (e.g., see Fig. 3), with rapid transitions between high-FRET/low-FRET states denoting distance changes between P1-P5 moieties of the riboswitch (56). It is worth noting that multiple open conformations (e.g., any open/unbound state [O] or the ligand bound state [O·Lys]) are detected equivalently as low FRET states, only some of which may bind lysine and subsequently successfully fold. The biophysical implication of distributions in open states is considered in the results and discussion sections. FRET efficiency histograms for both BSU and TMA lysine riboswitches reveal two well-resolved states at $E_{\text{FRET}} \sim 0.3$ and 0.8, corresponding to the open (both O and O·Lys) and closed (both C and C·Lys) conformations. The threshold for distinguishing these two conformations is taken as the local minimum in such FRET histograms, which permits dwell times for folding/unfolding events to be quantitatively extracted from the trajectories. This sequence of dwell times is used to construct cumulative distribution functions well-fit by single exponential unimolecular folding (k_{fold}) and unfolding (k_{unfold}) rate constants and consistent with a single rate-limiting transition state (56,62,68). Equilibrium constants are calculated from $K_{\text{eq}} = k_{\text{fold}}/k_{\text{unfold}}$ or by the ratio of integrated fractional time spent in open versus closed conformations, which in all cases agrees with the reported rate constant ratios to within experimental uncertainty.

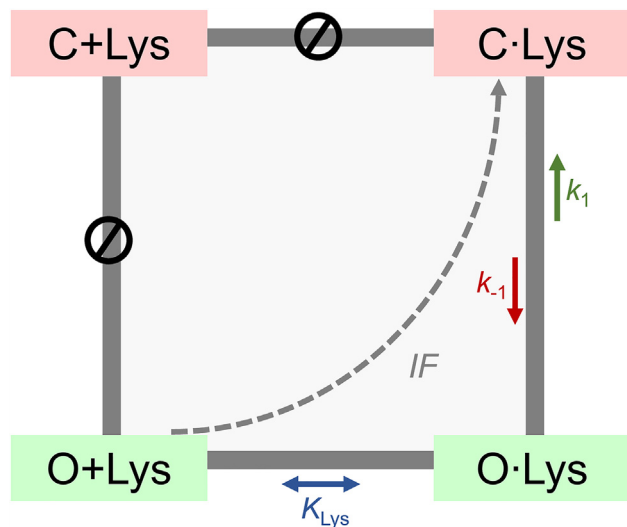


FIGURE 4 A four-state (i.e., “square”) model for riboswitch folding allows for the riboswitch to be in ligand bound/unbound and open/closed states. The induced-fit (IF), or “bind-then-fold,” model requires that the ligand bind before folding, omitting the unbound, closed state, which leaves three states: $O + \text{Lys} \rightleftharpoons O \cdot \text{Lys} \rightleftharpoons C \cdot \text{Lys}$. The $O + \text{Lys}$ and $O \cdot \text{Lys}$ states are experimentally indistinguishable and register as low-FRET (green), while the $C \cdot \text{Lys}$ state registers as high-FRET (red).

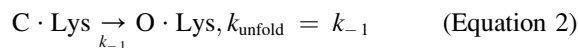
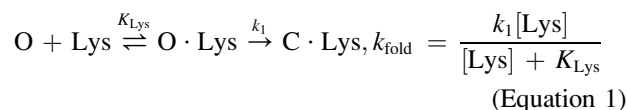
RESULTS

TMA and BSU riboswitches both fold via an IF (bind-then-fold) mechanism

We first explore the differences and similarities in BSU/TMA riboswitch behavior by comparison of the single-molecule folding kinetics. Specifically, the mesophilic BSU lysine riboswitch has been shown previously to fold via a predominantly IF (bind-then-fold) mechanism as depicted by the counterclockwise arc in Fig. 4, in which the riboswitch must first bind to lysine in the open state ($O + \text{Lys} \rightleftharpoons O \cdot \text{Lys}$) before folding occurs ($O \cdot \text{Lys} \rightleftharpoons C \cdot \text{Lys}$) (56). The kinetic signature of such an IF pathway is that it depends on a *bimolecular* lysine-dependent equilibrium between open lysine-unbound ($O + \text{Lys}$) and lysine-bound ($O \cdot \text{Lys}$) states before folding (i.e., $O \rightarrow C$, closing), while unfolding (i.e., $C \rightarrow O$, opening) occurs via a *unimolecular* equilibration step ($C \cdot \text{Lys} \rightleftharpoons O \cdot \text{Lys}$). In agreement with this model, both BSU and TMA exhibit strong lysine-dependent kinetics for k_{fold} but negligible lysine dependence for k_{unfold} (see Fig. 5, *a* and *b*), indicating that BSU and TMA riboswitches each require lysine binding before folding. Thus, folding in both mesophilic and thermophilic constructs follows a classic IF (bind-then-fold) kinetic pathway that requires lysine to fold, as described previously (56,57), and has $k_{\text{fold}} = 0 \text{ s}^{-1}$ at $[\text{Lys}] = 0 \text{ mM}$.

We can further probe the lysine dependence of this IF kinetic folding pathway to determine the lysine dissociation constants K_{Lys} for each riboswitch. To do so, we would ideally fit the folding (i.e., closing) and unfolding rate

data under identical salt concentrations to the following mechanisms:



However, as mentioned previously, the measured unfolding rates at a given $[\text{K}^+]$ are dramatically slower (and folding rates considerably faster) for TMA than BSU (see Fig. 3). As a result, it is not possible with our current experimental methods to compare the BSU and TMA folding/unfolding behavior under the same cation conditions, since the predicted timescales for folding in BSU (or unfolding in TMA) exceed the maximum photobleaching times at low (or high) $[\text{K}^+]$. Instead, we compare $[\text{Lys}]$ -dependent data for both riboswitches at fixed $[\text{Na}^+] = 100 \text{ mM}$, $[\text{Mg}^{2+}] = 0.5 \text{ mM}$, but different $[\text{K}^+]$: specifically, 5 and 75 mM for TMA and BSU, respectively. Even under these $15\times$ higher $[\text{K}^+]$ conditions, the data in Fig. 5, *a* and *b* reveal the BSU-lysine complex to still be $6\times$ less stable than for TMA: $K_{\text{Lys}} = 4(1) \text{ mM}$ (BSU) vs. $0.6(1) \text{ mM}$ (TMA). Indeed, previous studies in BSU have suggested that increase in $[\text{K}^+]$ from 1 to 10 mM enhances lysine binding by mediating Coulombic repulsion between the negatively charged lysine carboxylate and the phosphate backbone (34,69). This would be consistent with smaller dissociation constants for TMA at higher $[\text{K}^+]$ (75 mM K^+ in BSU vs. 5 mM K^+ in TMA), again confirming the much tighter binding of lysine with TMA vs. BSU at room temperature. While these dissociation constants are consistent with previous FRET-based measurements, they differ from titration dialysis and isothermal calorimetry measurements that find $K_{\text{Lys}} = 1\text{--}18 \mu\text{M}$ for BSU (40,70) and $K_{\text{Lys}} = 5.5 \mu\text{M}$ for TMA (34). However, these lower dissociation constants were determined at $[\text{Mg}^{2+}] = 5\text{--}20 \text{ mM}$, while our measurements are taken at much lower $[\text{Mg}^{2+}] = 0.5 \text{ mM}$, which often results in higher dissociation constants/weaker lysine binding (30,71).

BSU and TMA folding is exothermically ($\Delta H < 0$) and entropically ($\Delta S > 0$) costly

Previous studies have reported BSU riboswitch folding to be significantly exothermic ($\Delta H = -20\text{--}40 \text{ kcal/mol}$) (57), which from Le Chatelier’s principle predicts a strong decrease in folding stability with increasing temperature. Given that the two riboswitch constructs function in quite different temperature environments (40 vs. 80°C , respectively), this raises the interesting thermodynamic question as to how efficient ligand binding is managed in TMA versus BSU. To help address such questions, we have studied the kinetics of BSU and TMA folding as a function of

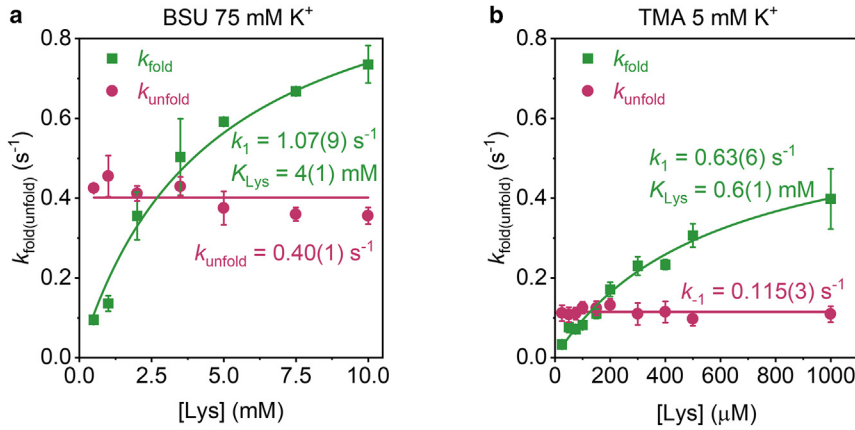


FIGURE 5 Lysine binding curves for the (a) BSU riboswitch at 75 mM K^+ and (b) TMA riboswitch at 5 mM K^+ . Error bars in parentheses represent standard deviations of the mean obtained from analysis of 3 independent datasets. Both samples contain 100 mM Na^+ and 0.5 mM Mg^{2+} and were collected at 23°C. Folding in both is strongly [Lys] dependent, while unfolding has no [Lys] dependence, which indicates an induced-fit (bind-then-fold) folding mechanism for both riboswitches. Note that the TMA dissociation constant (K_{Lys}) is already $\sim 6\times$ lower than BSU, indicating a $6\times$ stronger lysine binding despite a $15\times$ reduction in $[K^+]$. For a more quantitative comparison, we therefore perform temperature-dependent TMA experiments at low $[K^+]$ and extrapolate the results to higher $[K^+]$.

temperature to extract explicit thermodynamic information (72) from the van't Hoff and Gibbs free energy expressions:

$$K_{eq} = \exp(-\Delta G^\circ / k_B T) \quad (\text{Equation 3})$$

$$\Delta G^\circ = \Delta H^\circ - T\Delta S^\circ \quad (\text{Equation 4})$$

$$\ln(K_{eq}) = -(\Delta H^\circ / k_B)(1/T) + \Delta S^\circ / k_B \quad (\text{Equation 5})$$

by which ΔH° is obtained from slopes ($-\Delta H^\circ/k_B$) of linear fits of $\ln(K_{eq})$ vs. $1/T$ and ΔS° is inferred from the corresponding intercepts ($\Delta S^\circ/k_B$). Although our temperature-dependent data for the BSU and TMA riboswitches are measured for different $[K^+]$, Fig. 6 a clearly reveals good qualitative agreement between the two constructs, both folding processes are strongly exothermic (slopes $\gg 0$) and with large entropic penalties (intercepts $\ll 0$).

Furthermore, examination of the temperature-dependent smFRET kinetics permit additional characterization of the transition state thermodynamics based on Eyring/Kramers analysis (73) of the folding/unfolding rate constants:

$$\ln(k_{fold(unfold)}) = (-\Delta G^\ddagger) / k_B T + \ln(\kappa\nu_o) = -\Delta H^\ddagger / k_B T + \Delta S^\ddagger / k_B + \ln(\kappa\nu_o) \quad (\text{Equation 6})$$

Here, slopes ($-\Delta H^\ddagger/k_B$) from linear fits of $\ln(k_{fold(unfold)})$ vs. $1/T$ yield transition state enthalpies, while the intercepts ($\Delta S^\ddagger/k_B + \ln(\kappa\nu_o)$) reveal transition state entropies offset by attempt frequency (ν_o) and barrier recrossing (κ) terms. For conformational transformation in large biomolecules, $\kappa\nu_o$ is conventionally approximated as 10^6-10^8 s^{-1} , although ΔS^\ddagger has only a weak (i.e., logarithmic) dependence on this assumption. It is worth noting that such choices do not impact differential changes in the transition state entropy, which means that $\Delta\Delta S^\ddagger$ values are determined absolutely and can be used to compare TMA and BSU thermodynamics directly.

Plots of temperature-dependent rate constants are summarized in Fig. 6 and reveal both BSU and TMA riboswitches to incur strong entropic penalties ($-\Delta\Delta S^\ddagger > 0$) compensated by strong enthalpic release ($\Delta\Delta H^\ddagger < 0$) in approaching the transition state, as evident in both $O \rightarrow TS$ (\ddagger) (Fig. 6, a and b, green) and $C \rightarrow TS$ (\ddagger) (Fig. 6, red) directions. To visually deconstruct these free energy barrier contributions, the temperature-dependent data are represented in Fig. 7 as separate ΔH , ΔS , and ΔG thermodynamic landscapes. Interestingly, data for both BSU and TMA riboswitches are consistent with folding pathways in which approximately half of the key enthalpic contacts are already formed in achieving the forward transition state geometry (BSU: $\Delta H^\ddagger \sim 40\% \Delta H^\circ$; TMA: $\Delta H^\ddagger \sim 60\% \Delta H^\circ$), but where the clear majority of entropy loss due to structural reorganization has already taken place (BSU: $\Delta S^\ddagger \sim 70\% \Delta S^\circ$; TMA: $\Delta S^\ddagger \sim 80\% \Delta S^\circ$). This is again consistent with previous work that shows BSU folding requires only a fraction of the full complement of H-bonds to be formed between lysine and aptamer domain and within the aptamer domain in order for the riboswitch to recognize the ligand and then trigger the resulting conformational rearrangement. Most importantly, when ΔG^\ddagger is calculated at relevant environmental temperatures for BSU (40°C) and TMA (80°C), this results in large free energy TS barriers to folding for both, $\Delta G^\ddagger = 10(2)$ kcal/mol (BSU) and $14(2)$ kcal/mol (TMA), despite much more modest overall ΔG° (2.5(2) kcal/mol (BSU) and 6.2(3) kcal/mol (TMA)). Finally, because overall folding is clearly exothermic for both BSU and TMA riboswitches, this raises the question of how these two riboswitches compensate for quite different ambient temperature environments.

Agreement between BSU and TMA thermodynamics for extrapolated $[K^+]$ conditions

Despite fivefold differences in $[K^+]$, the kinetic and thermodynamic data for BSU and TMA riboswitches exhibit qualitatively similar ligand binding and folding/unfolding

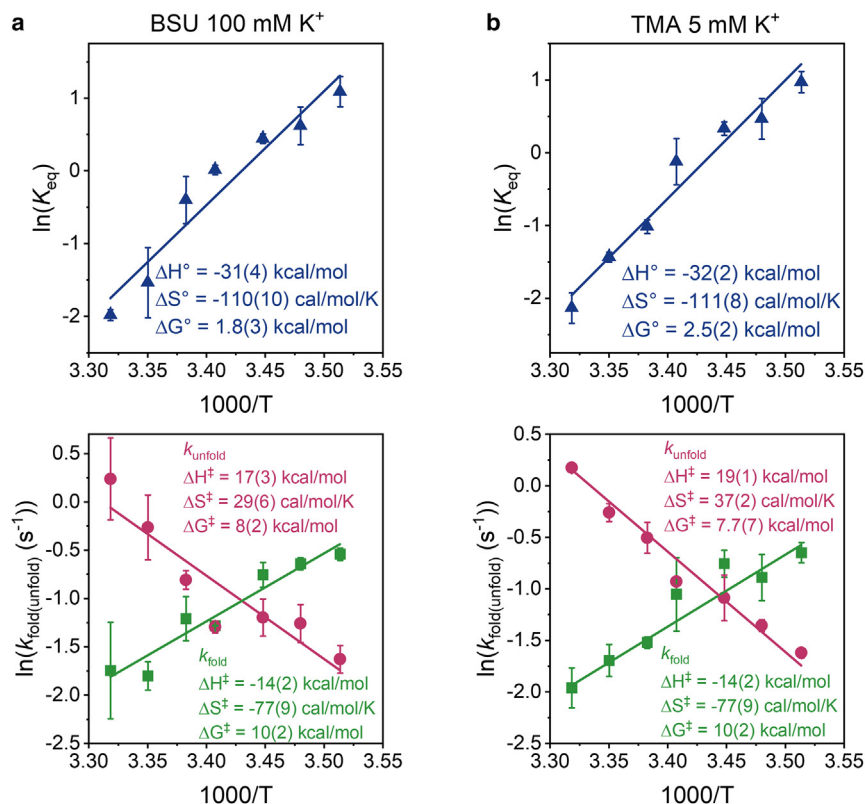


FIGURE 6 van't Hoff (*top*) and Eyring (*bottom*) plots for (a) BSU and (b) TMA riboswitches at 100 and 5 mM K⁺, respectively. Both van't Hoff plots have positive slopes and negative intercepts, which indicates exothermic ($\Delta H^\circ < 0$) and entropically costly ($\Delta S^\circ < 0$) folding thermodynamics for both BSU and TMA. From a similar Eyring analysis of the temperature-dependent rate constants, the plots (*lower panels*) reveal that the O + Lys \rightarrow TS step is exothermic and entropically unfavorable, while the C·Lys \rightarrow TS step is endothermic and entropically favorable. As a result, folding processes proceeding along the O + Lys \rightarrow TS \rightarrow C·Lys reaction coordinate are therefore exothermic and entropically costly at each step. Both samples contain 100 mM Na⁺ and 0.5 mM Mg²⁺ and are calculated at 300 K. Error bars in parentheses represent standard deviations of the mean obtained from analysis of 3 independent datasets.

kinetics in Fig. 7. In both riboswitches, lysine binding precedes conformational change, with free energy landscapes revealing both enthalpic advantages and entropic penalties to reach the TS (\ddagger) as well as the closed conformation. To help make such comparisons more quantitative, however, we have performed additional temperature-dependent experiments for the TMA riboswitch over a systematic series of [K⁺] = 1, 2, 5, 10, and 20 mM but for fixed [Na⁺] = 100 mM, [Mg²⁺] = 0.5 mM, and [Lys] = 2 mM concentrations (59). Basically, these conditions reflect a [K⁺] concentration range that allows multiple (>10) folding/unfolding events for each RNA molecule to ensure sufficiently good

statistics before photobleaching occurs. We compensate for any reduction in total event number by observing a proportionally larger number of single-molecule constructs, and thereby ensure that any photobleaching contributions to the rate constant measurements is small (<10%) with respect to the reported uncertainties. We then use data from this [K⁺] range to extrapolate the TMA enthalpy and entropy of folding to directly compare BSU and TMA behavior at 100 mM K⁺ in Fig. 8. By way of a zeroth-order model for potassium ions taken into or released from the binding pocket in each folding/unfolding event, we expect (e.g., the work of Record et al. (74)) the enthalpic/entropic

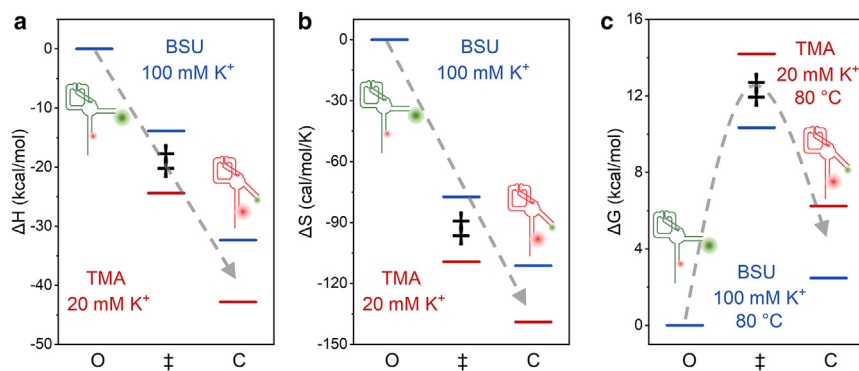


FIGURE 7 Energy landscapes for the BSU riboswitch at 100 mM K⁺ and TMA riboswitch at 20 mM K⁺. For both riboswitches, folding is (a) enthalpically favorable: $\Delta H^\ddagger = -24(2)$ kcal/mol TMA, $-13(2)$ kcal/mol BSU; $\Delta H^\circ = -42(1)$ kcal/mol TMA, $-32(2)$ kcal/mol BSU, (b) entropically costly throughout the entire reaction coordinate: $\Delta S^\ddagger = -110(10)$ cal/mol/K TMA, $-77(8)$ cal/mol/K BSU; $\Delta S^\circ = -139(5)$ cal/mol/K TMA, $-111(8)$ cal/mol/K BSU, and results in (c) a large transition state barrier ($\Delta G^\ddagger = 14(2)$ kcal/mol TMA, $10(2)$ kcal/mol BSU) to folding despite a much more modest overall change in free energy ($\Delta G^\circ = 6.2(3)$ kcal/mol TMA, $2.5(2)$ kcal/mol BSU). Error bars in parentheses represent standard deviations of the mean obtained from analysis of 3 independent datasets.

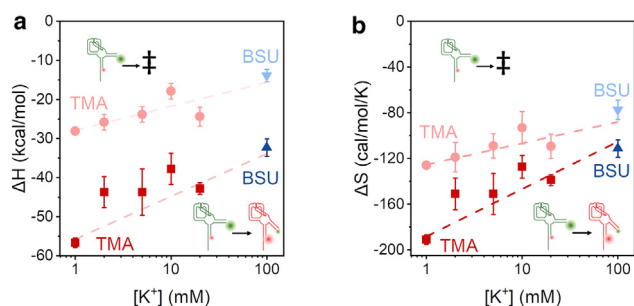


FIGURE 8 (a) Enthalpic and (b) entropic contributions to folding from the O + Lys state to the TS (light colors, top traces) and the lysine bound/closed C·Lys state (dark colors, bottom traces). Error bars in parentheses represent standard deviations of the mean obtained from analysis of 3 independent datasets. For comparison, the BSU data at $[K^+] = 100$ mM are represented by dark blue ($\Delta H^\circ/\Delta S^\circ$) and light blue triangles ($\Delta H^\ddagger/\Delta S^\ddagger$), with the TMA data in red squares ($\Delta H^\circ/\Delta S^\circ$) and pink circles ($\Delta H^\ddagger/\Delta S^\ddagger$). Fits to the low $[K^+]$ TMA data are linearly extrapolated and exhibit nearly quantitative agreement with BSU data at 100 mM K^+ (see Table 1 for full comparison). Error bars in parentheses represent standard deviations of the mean obtained from analysis of 3 independent datasets.

contributions to be linearly dependent on chemical potential (μ_{K^+}) and thus $\ln[K^+]$. We therefore utilize linear extrapolation in $\ln[K^+]$ of the TMA enthalpy and entropy contributions to facilitate a more quantitative comparison with our BSU folding studies at 100 mM K^+ .

Fig. 8 summarizes all ΔH (Fig. 8 a) and ΔS (Fig. 8 b) data plotted against $\ln[K^+]$ for $[K^+] = 1, 2, 5, 10,$ and 20 mM for TMA (red) and $[K^+] = 100$ mM BSU (blue) for the forward $U \rightarrow TS$ (light color) and overall $U \rightarrow F$ (dark color) folding kinetics. These $[K^+]$ values again fall into a range where folding and unfolding kinetics are experimentally feasible to measure for TMA. As expected, the plots for TMA (Fig. 8 a) are in good agreement with a linear dependence of ΔH° and ΔH^\ddagger on $\ln[K^+]$, with similar semilogarithmic linearity with respect to $\ln[K^+]$ indicated in the corresponding plots (Fig. 8 b) for ΔS° and ΔS^\ddagger . Quite notably, the TMA extrapolated results for both ΔH and ΔS are within reported uncertainties for the corresponding BSU riboswitch ΔH and ΔS values experimentally measured at 100 mM K^+ (see Table 1). This is unexpected but consistent with energetically similar interactions between lysine and the two riboswitches as well as similar conformational changes between open and closed states. More surprisingly, however, ΔH and ΔS both increase with increasing $[K^+]$ (1–20 mM) for TMA (Fig. 8, a and b), which is notably different from the corresponding decrease in ΔH and ΔS with $[K^+]$ reported previously for the BSU ri-

TABLE 1 Enthalpy and entropy of folding in TMA and BSU aptamers at 100 mM K^+

	ΔH^\ddagger (kcal/mol)	ΔH° (kcal/mol)	ΔS^\ddagger (cal/mol/K)	ΔS° (cal/mol/K)
TMA (extrapolated)	-16(6)	-34(9)	-88(26)	-105(25)
BSU (measured)	-14(2)	-32(2)	-77(8)	-111(8)

boswitch (69). In attempting to rationalize these opposing trends, it still seems quite likely that potassium plays a role as bridge cation between the carboxylic acid group in lysine and the negatively charged RNA, as indeed is evident in the x-ray crystal structure of the TMA binding pocket. However, one could also speculate that higher $[K^+]$ may displace waters tightly bound to the phosphate backbone or even displace or compete with lysine in the binding pocket. This could result in changes to the RNA solvation shell and interruptions in hydrogen bonds between the RNA, water, and lysine essential to maintain riboswitch secondary and tertiary structure.

The ΔH and ΔS values in Fig. 8 can be used to construct similar extrapolation plots of free energies for the transition state (ΔG^\ddagger) and overall folding (ΔG°) at 80 and 40°C for TMA and BSU, respectively. Transition state free energies (ΔG^\ddagger) (see Fig. 9 a) for TMA indicate only a modest $[K^+]$ -dependent decrease over the same potassium range (1, 2, 5, 10, 20 mM, in light red), with the TMA extrapolation of ΔG^\ddagger to 100 mM K^+ quite comparable with that of BSU (13(2) and 10(2) kcal/mol, respectively). The ΔG° data (Fig. 9, a and b, dark red) exhibit a significantly steeper dependence on $\ln[K^+]$, although once again the extrapolated 100 mM K^+ values for BSU and TMA (2.5(2) and 3.8(2) kcal/mol, respectively) are quite comparable. This comparison implies a greater potassium cation induced stability for overall folding of the TMA riboswitch, although with clearly lower $[K^+]$ sensitivity in the forward (folding) versus reverse (unfolding) rate constants. The key result is that temperature- and $[K^+]$ -extrapolated ΔG^\ddagger and ΔG° values for BSU and TMA riboswitches are within ~ 1 –2 kcal/mol of each other at their respective ambient functional temperatures (40 vs. 80°C), i.e., much less than the free energy of a typical hydrogen bonding interaction.

DISCUSSION

BSU and TMA exhibit similar folding mechanisms and energetic contributions to folding

Lysine strongly influences both BSU and TMA folding rate constants with virtually no effect on the unfolding rates, consistent with lysine binding to the aptamer domain before conformational changes to the riboswitch take place (i.e., IF kinetics). From the temperature-dependent single-molecule studies, van't Hoff and Eyring analysis reveals that equilibrium (K_{eq}) and folding rate constants (k_{fold}) decrease with temperature while unfolding rate constants (k_{unfold}) increase with temperature for both riboswitch constructs. The thermodynamic folding landscapes for both BSU and TMA riboswitches are enthalpically favorable yet entropically costly for each of the pathways from 1) open to transition state ($\Delta H^{O \rightarrow \ddagger} < 0$, $\Delta S^{O \rightarrow \ddagger} < 0$), 2) transition state to closed ($\Delta H^{\ddagger \rightarrow C} < 0$, $\Delta S^{\ddagger \rightarrow C} < 0$), and thus for 3) the overall folding process itself ($\Delta H^\circ < 0$, $\Delta S^\circ < 0$). Furthermore, the considerable majority of any entropic changes in the riboswitch conformation take place before the transition state

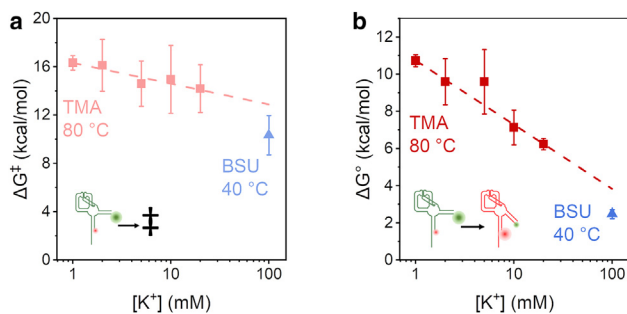


FIGURE 9 (a) Transition state (ΔG^\ddagger) and (b) overall (ΔG°) free energy changes for BSU (blue triangles) and TMA (red squares) calculated at environmentally appropriate 40 and 80°C temperatures, respectively. Despite significant differences in biological operating temperature, fits to low $[K^+]$ TMA data linearly extrapolated to 100 mM K^+ yield values in reasonable agreement with the BSU results: ΔG^\ddagger (10(2) vs. 13(2) kcal/mol) and ΔG° (2.5(2) vs. 3.8(2) kcal/mol). Error bars in parentheses represent standard deviations of the mean obtained from analysis of 3 independent data sets.

($\Delta S^{O \rightarrow \ddagger} = -77(8)/-88(26)$ cal/mol/K vs. $\Delta S^\circ = -111(8)/-105(25)$ cal/mol/K), despite releasing only $\sim 50\%$ of the bond enthalpy ($\Delta H^{O \rightarrow \ddagger} = -14(2)/-16(6)$ kcal/mol vs. $\Delta H^\circ = -32(2)/-34(9)$ kcal/mol) for BSU/TMA, respectively. The competition between these two thermodynamic effects results in a large transition state barrier ($\Delta G^{O \rightarrow \ddagger} = 10(2)/13(2)$ kcal/mol for BSU/TMA at 300 K) yet only a slightly unfavorable overall free energy folding ($\Delta G^\circ = 2.5(2)/3.8(2)$ kcal/mol for BSU/TMA at 300 K). Moreover, the $\ln[K^+]$ linearly extrapolated ΔH and ΔS thermodynamic values for TMA and BSU match at near physiological $[K^+] = 100$ mM concentrations. This suggests that, once in the correct open state for which the crucially important P2-P3 and P2-P4 tertiary interactions have been achieved, further progress along the folding coordinate for both riboswitches involves similar ligand binding between lysine/potassium and the RNA aptamer, changes in the riboswitch tertiary conformation (largely P1-P5), accompanied by solvent reorganization. Finally, the quantitative values for ΔH and $-\Delta S$ are such that transition state and overall free energies remain nearly balanced, all of which permit the TMA and BSU riboswitches to remain biocompetent in regulating gene expression over a significantly broad ($T = 40\text{--}80^\circ\text{C}$) range of environmental temperatures.

Folding/unfolding rates for TMA and BSU agree at environmental temperature conditions

In addition to deconstructing free energy contributions to folding into enthalpic and entropic components, temperature-dependent analysis of the riboswitch kinetics similarly permits a more quantitative comparison of folding/unfolding rate constants for BSU at 40°C and TMA at 80°C. To obtain such predictions, we first extrapolate the van't Hoff/Eyring fits in Fig. 6 to determine the K_{eq} , k_{fold} , and

k_{unfold} values at their respective temperatures for the same salt conditions. That is, we extrapolate to predict K_{eq} , k_{fold} , and k_{unfold} for TMA at 80°C and $[K^+] = 1, 2, 5, 10,$ and 20 mM and for BSU at 40°C and $[K^+] = 100$ mM (see Fig. 10, extrapolated values are hollow). It is worth noting that such a linear extrapolation in $\ln[K^+]$ assumes negligible changes in heat capacity due to folding (ΔC_P° and $\Delta C_P^\ddagger \approx 0$), where ΔC_P° and ΔC_P^\ddagger are related to changes in solvent-accessible surface area and thus reflect folding dependent changes in system-solvent interactions. In nucleic acid duplex formation, finite ΔC_P° or ΔC_P^\ddagger values can result from changes in polar/nonpolar group exposure to the solvent and even detectable in some systems by curvature in the van't Hoff/Eyring plots (75). In BSU/TMA riboswitches, however, all secondary and many of the important tertiary interactions (P2-P3, P2-P4) already exist before lysine binding, and folding is not thought to create any new secondary structure formation. Riboswitch solvation shells should therefore not be impacted by exposure and/or burial of polar/nonpolar regions during ligand binding and folding, but rather water and ion redistribution around existing RNA structures. Finally and most of all empirically, the van't Hoff data do not signal significant deviations from linear fits, either in this (see Fig. 10) or previous work (57,69), which we take as justifying neglect of ΔC_P° and ΔC_P^\ddagger in folding for the BSU and TMA lysine riboswitches within experimental uncertainty.

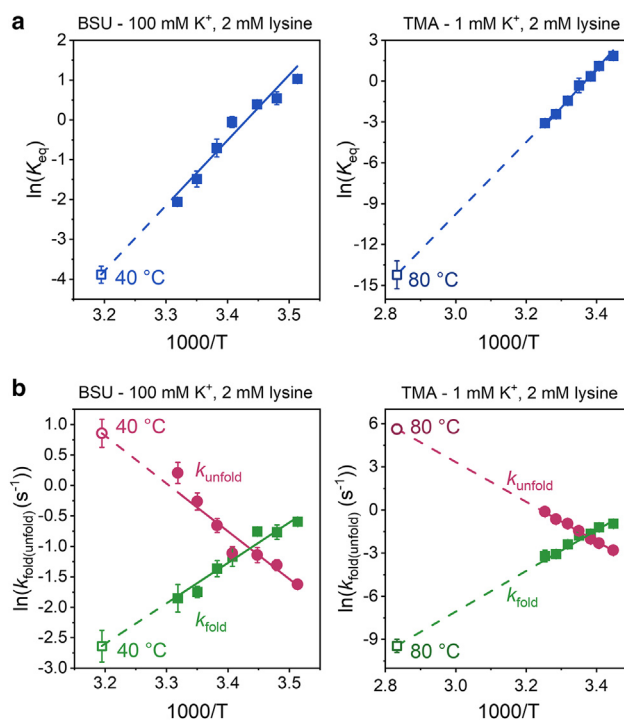


FIGURE 10 (a) van't Hoff and (b) Eyring plots at 100 mM (BSU) and 1 mM K^+ (TMA) with temperature extrapolated to determine K_{eq} and $k_{fold/unfold}$ at 40°C (BSU) and 80°C (TMA). Solid data points are experimentally determined; hollow data points represent extrapolations from a linear fit. Error bars in parentheses represent standard deviations of the mean obtained from analysis of 3 independent datasets.

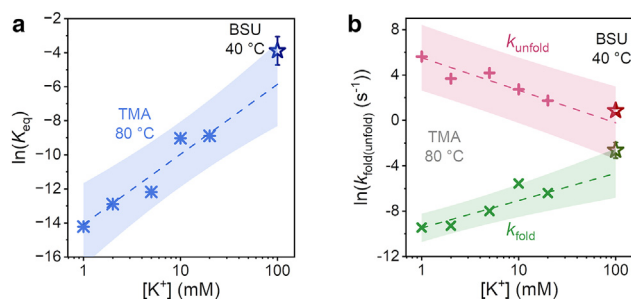


FIGURE 11 Extrapolated comparison of BSU and TMA K_{eq} , $k_{fold/unfold}$ values to their respective physiological temperatures: 40°C (BSU) and 80°C (TMA). (a) BSU (hollow star) and TMA (*) equilibrium constants and (b) BSU (hollow stars) and TMA (green x's/pink +'s) folding/unfolding rate constants, with shaded bands representing 2s (95%) uncertainties. The results support that low- $[K^+]$ TMA values can be logarithmically extrapolated to 100 mM K^+ to reveal K_{eq} and $k_{fold/unfold}$ values in reasonable agreement with BSU values at 100 mM K^+ .

Based on this approximation, we can then also extrapolate the 80°C K_{eq} , k_{fold} , and k_{unfold} values for TMA from Fig. 10 as a logarithmic function of potassium concentration (1, 2, 5, 10, and 20 mM K^+) to construct log-log plots of $\ln(K_{eq})$ and $\ln(k_{fold(unfold)})$ vs. $\log([K^+])$ shown in Fig. 11. This treatment is closely coupled to the extrapolations performed in Fig. 9, since K_{eq} , $k_{fold(unfold)}$ are exponentially related to ΔG° and ΔG^\ddagger , respectively. As expected (74), the equilibrium and rate constant data for TMA at 80°C are again both well described by a linear fit (see Fig. 11) and can be directly compared with the corresponding BSU data at 40°C and 100 mM K^+ in Table 2. Even more relevant to biochemical function, typical transcription rates for RNA polymerase ($\sim 20\text{--}60$ nt/s (76)) predict the overall ~ 50 nt expression platform domain (40) to be transcribed on the few seconds timescale, i.e., comparable with or even longer than the subsecond timescales predicted for achieving structural equilibration ($1/(k_{fold}+k_{unfold}) \sim 0.3\text{--}1$ s) of the riboswitch. The data therefore importantly predict that, under their respective environmental temperature and salt conditions, TMA and BSU riboswitches both can exhibit cotranscriptional lysine binding and conformational change on thermodynamically (versus kinetically) controlled timescales.

Structural differences in TMA versus BSU compensate for higher environmental temperature

Despite the higher-temperature operating environment, ligand binding and aptamer conformational change in the

TABLE 2 Folding/unfolding rates and equilibrium constants for TMA and BSU aptamers at 100 mM K^+ and environmental temperatures

	k_{fold} (s^{-1})	k_{unfold} (s^{-1})	K_{eq}
TMA (80°C)	0.07(1)	1.1(2)	0.0038(5)
BSU (40°C)	0.07(2)	2.4(5)	0.021(4)

TMA riboswitch still rely on exothermic bond formation to promote the closed conformation. At first this seems surprising, as exothermicity implies a decrease in riboswitch folding stability at higher temperatures and thus potentially limits gene regulation. It is worth noting that this is not always the case, as demonstrated in the *yybP-ykoY* manganese riboswitch (77), for which the free energy to spontaneous folding arises primarily from entropically favorable disorder of the solvent rather than enthalpically favorable bond formation between RNA and the ligand. This allows the entropic advantage ($-T\Delta S < 0$) to compensate for enthalpic penalty ($\Delta H > 0$), thereby achieving thermodynamic stability that increases with elevated temperature. For the present case of TMA and BSU lysine riboswitches, however, it appears that the strategy for high-temperature compensation is based on many small changes to the RNA primary sequence and possibly tertiary structure. Specifically, there is a notable increase in G-C basepair percentage (76% in TMA vs. 44% in BSU) which stabilizes the five helices comprising the riboswitch aptamer domain and in particular supports critical long-range P2-P3 kissing loop and the P2-P4 interactions, thereby protecting them from melting at the higher temperatures. These preserved tertiary interactions serve to prepare the riboswitch for ligand binding and, consequently, folding.

Importantly, we note that it is common for an increase in G-C basepair content to be combined with other high-temperature adaptations, since relying too heavily on increasing G-C basepairing can result in reduced structural diversity and an increased probability of misfolding (78). Indeed, previous studies of hyperthermophilic versus mesophilic species have revealed the importance of additional RNA tertiary interactions such as extra hydrogen bonds, internal-loop interactions, cross-strand purine stacking, and a variety of motifs that can tune the contact angle for important tertiary structures or adjust RNA compactness or flexibility (12,13). For example, temperature-gradient gel electrophoresis studies of the *Tetrahymena* ribozyme have shown that the most important mutations for high-temperature survival are those that increase tertiary interactions in the core of the structure or stabilize interactions between the different RNA domains but rarely increase GC content, even in basepaired regions (79).

Indeed, x-ray crystallography structure studies of the TMA lysine riboswitch reveal several tertiary interactions that may have a role in preserving function at high temperatures. While many lysine riboswitches, including BSU (55), use a kink-turn to achieve the correct orientation of the P2 terminal loop, the TMA version uses an internal loop motif to create the required 120° bend to form the P2-P3 kissing loop (48,49), which is critical in stabilizing the junction to correctly bind lysine. In addition, an unusual stacking interaction between G42 and U93 (see Fig. 1 b, blue circles) perpendicular to the P2 helical axis is thought to confer a crucial piece of extra stability to the P2-P3

element (48). The interaction between the P2 internal loop and the P4 terminal loop (P2-P4) is also stabilized by subtleties in tertiary structure; notably, the P4 U127 residue (see Fig. 1 *b*, orange circle) is flipped outward to create a GNRA tetraloop that interacts with the P2 minor groove, anchored by a U23A125G67 triple (see Fig. 1 *b*, yellow circles). These and other such specialized tertiary interactions (80–82) may confer additional stability to the TMA riboswitch structure and ensure biocompetency at higher temperatures (82–84). Clearly detailed crystallographic data on other lysine riboswitches (e.g., BSU) and thermophilic/mesophilic riboswitch families would be extremely useful in helping identify which of these possible tertiary interaction mechanisms are the most critical and/or universal in protecting riboswitch functionality in high-temperature environments.

As a parting comment, although we experimentally sort the single-molecule trajectories into open or closed state episodes, it is important to note that low FRET observation does not distinguish between 1) an open state with significantly preformed secondary and/or tertiary structure and 2) an open state that cannot bind lysine and therefore close successfully. In fact, some open states available to the riboswitch prevent folding entirely, as demonstrated in previous studies that probed misfolding or blocking the formation of tertiary structures (56). Therefore, increasing the G-C basepair stability of an open (albeit “binding-competent”) TMA riboswitch conformation could enhance lysine binding and thereby increase k_{fold} and K_{eq} compared with BSU for similar temperatures and salt conditions, thereby promoting TMA function at elevated temperatures. Such a mechanism for ligand binding at different temperatures could similarly impact the unfolding dynamics, with the presence of greater G-C basepairing and stable, preexisting structures triggering a decrease in k_{unfold} for the lysine-bound, closed state. From such a perspective, the strategy of higher basepair count in the TMA riboswitch might be better interpreted as not stabilizing ligand binding directly, but rather enhancing the thermal stability of critical tertiary structures such as the P2-P3 kissing loop and P2-P4 loop-loop interactions. These structures can in turn support the central junction (i.e., the lysine binding pocket) with the ultimate effect of promoting lysine binding and, consequently, successful gene regulation. Most importantly, such a G-C basepair adaptive strategy offers additional flexibility in the entropic versus enthalpic thermodynamic landscapes to achieve desired performance for a specific riboswitch and highlights the importance of preexisting tertiary structures in riboswitch function.

Conclusions

TMA and BSU riboswitches have undergone adaptations in primary sequence with largely conserved secondary and tertiary structures that allow them to function under signifi-

cantly different temperature environments. We have studied these two lysine riboswitches with temperature-dependent single-molecule FRET microscopy to explore genetic adaptation between hyperthermophilic and mesophilic conditions and find surprisingly similar ligand binding strategies. In probing the lysine-dependent kinetics, we find that both TMA and BSU require lysine binding *before* the riboswitch switches conformation, i.e., an IF mechanism. In addition, thermodynamic landscapes for both riboswitches reveal that binding is an exclusively exothermic and entropically costly process in which entropic/enthalpic components compete to generate large transition state free energy barriers to folding, despite modest changes in overall free energy. Most importantly, the transition states in these riboswitches are both characterized by only partial release of the full bond formation exothermicity ($\Delta H^\ddagger \sim 45\% \Delta H^\circ$). In clear contrast, by the time these transition state barriers are crossed, the constructs have already paid the majority ($\Delta S^\ddagger \sim 70\text{--}80\% \Delta S^\circ$) of the entropic penalty required by conformational changes in the lysine-bound RNA. This suggests that only a few critical lysine-RNA contacts are necessary to trigger folding in each of the TMA and BSU riboswitches.

We also directly compare folding in these riboswitches by extrapolating TMA and BSU results to near physiological K^+ cation conditions to predict free energy contributions to folding for each riboswitch at their respective biological temperatures. This analysis reveals the enthalpic advantages ($\Delta H < 0$) and entropic penalties ($-\Delta S > 0$) to be in near quantitative agreement with each other at the same $[K^+]$, with free energies ΔG° s and ΔG^\ddagger s for TMA (80°C) and for BSU (40°C) within 1–2 kcal/mol. Finally, under the same salt conditions and at environmentally relevant temperatures, the TMA/BSU folding and unfolding rates are also predicted to be in good agreement. The study therefore reveals lysine-binding for both mesophilic (BSU) and thermophilic (TMA) riboswitches to be remarkably comparable and suggests that G-C basepair modifications are used to tune secondary and tertiary structure stability such that folding and unfolding can still occur on timescales commensurate with transcription. This provides at least one example of genetic adaptation to the environment that does not require major changes in ligand binding strategy to accommodate a large range of thermal conditions, but instead exploits multiple, smaller single basepair (e.g., G-C versus A-T) and tertiary structure modifications to allow the same riboswitch folding strategy to succeed in multiple biological windows of operation.

AUTHOR CONTRIBUTIONS

A.M.M. was responsible for the performing the reported research, collection and analysis of the data, as well as writing the initial draft and editing of the manuscript. The experimental research apparatus and program was

initially developed by D.J.N., who helped with research design/analysis as well as contributing to the writing/editing of the paper.

ACKNOWLEDGMENTS

Initial support for this work has been through the National Science Foundation (CHE 2053117) from the Chemical, Structure, Dynamics and Mechanisms-A Program, with recent transition support from the Air Force Office of Scientific Research (FA9550-15-1-0090) and additional funds for development of the TIRF apparatus from PHY-1734006/PHY-2317149 (Physics Frontier Center Program). We would like to express our sincere gratitude to Prof. Robert Batey (University of Colorado) for his careful reading of and valuable insights into the analysis and writing of the manuscript. We would also like to acknowledge early seed contributions by the W.M. Keck Foundation Initiative in RNA Sciences at the University of Colorado, Boulder.

DECLARATION OF INTERESTS

The authors declare no competing interests.

REFERENCES

- Siliakus, M. F., J. van der Oost, and S. W. M. Kengen. 2017. Adaptations of archaeal and bacterial membranes to variations in temperature, pH and pressure. *Extremophiles*. 21:651–670. <https://doi.org/10.1007/s00792-017-0939-x>.
- Kohli, I., N. C. Joshi, ..., A. Varma. 2020. Extremophile - an adaptive strategy for extreme conditions and applications. *Curr. Genom.* 21:96–110. <https://doi.org/10.2174/1389202921666200401105908>.
- Silva, B., C. Antunes, ..., A. T. Luís. 2021. Prokaryotic and eukaryotic diversity in hydrothermal continental systems. *Arch. Microbiol.* 203:3751–3766. <https://doi.org/10.1007/s00203-021-02416-1>.
- Stetter, K. O. 1999. Extremophiles and their adaptation to hot environments. *FEBS Lett.* 452:22–25. [https://doi.org/10.1016/S0014-5793\(99\)00663-8](https://doi.org/10.1016/S0014-5793(99)00663-8).
- Tamby, A., J. S. S. Damste, and L. Villanueva. 2023. Microbial membrane lipid adaptations to high hydrostatic pressure in the marine environment. *Front. Mol. Biosci.* 9:11. <https://doi.org/10.3389/fmolb.2022.1058381>.
- Feder, M. E., and G. E. Hofmann. 1999. Heat-shock proteins, molecular chaperones, and the stress response: Evolutionary and ecological physiology. *Annu. Rev. Physiol.* 61:243–282. <https://doi.org/10.1146/annurev.physiol.61.1.243>.
- Narberhaus, F. 2010. Translational control of bacterial heat shock and virulence genes by temperature-sensing mRNAs. *RNA Biol.* 7:84–89. <https://doi.org/10.4161/rna.7.1.10501>.
- Sharma, A., H. K. Alajangi, ..., R. P. Barnwal. 2022. RNA thermometers and other regulatory elements: Diversity and importance in bacterial pathogenesis. *Wiley Interdiscip. Rev. RNA*. 13:e1711. <https://doi.org/10.1002/wrna.1711>.
- Breaker, R. R. 2012. Riboswitches and the RNA world. *Cold Spring Harbor Perspect. Biol.* 4:a003566. <https://doi.org/10.1101/cshperspect.a003566>.
- Husser, C., N. Dentz, and M. Ryckelynck. 2021. Structure-switching RNAs: From gene expression regulation to small molecule detection. *Small Struct.* 2. <https://doi.org/10.1002/sstr.202000132>.
- Serganov, A. 2009. The long and the short of riboswitches. *Curr. Opin. Struct. Biol.* 19:251–259. <https://doi.org/10.1016/j.sbi.2009.02.002>.
- Grosjean, H., and T. Oshima. 2007. How nucleic acids cope with high temperature. In *Physiology and Biochemistry of Extremophiles*, pp. 39–56.
- Baird, N. J., N. Srividya, ..., T. Pan. 2006. Structural basis for altering the stability of homologous RNAs from a mesophilic and a thermophilic bacterium. *RNA*. 12:598–606. <https://doi.org/10.1261/rna.2186506>.
- Bringer, C., S. Spradlin, ..., C. Evilia. 2018. The more adaptive to change, the more likely you are to survive: Protein adaptation in extremophiles. *Semin. Cell Dev. Biol.* 84:158–169. <https://doi.org/10.1016/j.semcdb.2017.12.016>.
- Bowers, K. J., N. M. Mesbah, and J. Wiegel. 2009. Biodiversity of poly-extremophilic bacteria: Does combining the extremes of high salt, alkaline pH and elevated temperature approach a physico-chemical boundary for life? *Saline Syst.* 5:9. <https://doi.org/10.1186/1746-1448-5-9>.
- Martin, A., and A. McMinn. 2017. Sea ice, extremophiles and life on extra-terrestrial ocean worlds. *Int. J. Astrobiol.* 17:1–16. <https://doi.org/10.1017/S1473550416000483>.
- Littlechild, J. A. 2015. Enzymes from extreme environments and their industrial applications. *Front. Bioeng. Biotechnol.* 3:161. <https://doi.org/10.3389/fbioe.2015.00161>.
- van den Burg, B. 2003. Extremophiles as a source for novel enzymes. *Curr. Opin. Microbiol.* 6:213–218. [https://doi.org/10.1016/S1369-5274\(03\)00060-2](https://doi.org/10.1016/S1369-5274(03)00060-2).
- Demirjian, D. C., F. Morís-Varas, and C. S. Cassidy. 2001. Enzymes from extremophiles. *Curr. Opin. Chem. Biol.* 5:144–151. [https://doi.org/10.1016/S1367-5931\(00\)00183-6](https://doi.org/10.1016/S1367-5931(00)00183-6).
- Pavlova, N., D. Kaloudas, and R. Penchovsky. 2019. Riboswitch distribution, structure, and function in bacteria. *Gene*. 708:38–48. <https://doi.org/10.1016/j.gene.2019.05.036>.
- McCown, P. J., K. A. Corbino, ..., R. R. Breaker. 2017. Riboswitch diversity and distribution. *RNA*. 23:995–1011. <https://doi.org/10.1261/rna.061234.117>.
- Kulshina, N., T. E. Edwards, and A. R. Ferré-D'Amaré. 2010. Thermodynamic analysis of ligand binding and ligand binding-induced tertiary structure formation by the thiamine pyrophosphate riboswitch. *RNA*. 16:186–196. <https://doi.org/10.1261/rna.1847310>.
- Speed, M. C., B. W. Burkhardt, ..., T. J. Santangelo. 2018. An archaeal fluoride-responsive riboswitch provides an inducible expression system for hyperthermophiles. *Appl. Environ. Microbiol.* 84:e02306-17. <https://doi.org/10.1128/aem.02306-17>.
- Croft, M. T., M. Moulin, ..., A. G. Smith. 2007. Thiamine biosynthesis in algae is regulated by riboswitches. *Proc. Natl. Acad. Sci. USA*. 104:20770–20775. <https://doi.org/10.1073/pnas.0705786105>.
- Ariza-Mateos, A., A. Nuthanakanti, and A. Serganov. 2021. Riboswitch mechanisms: New tricks for an old dog. *Biochemist.* 86:962–975. <https://doi.org/10.1134/s0006297921080071>.
- Tucker, B. J., and R. R. Breaker. 2005. Riboswitches as versatile gene control elements. *Curr. Opin. Struct. Biol.* 15:342–348. <https://doi.org/10.1016/j.sbi.2005.05.003>.
- Bédard, A. S. V., E. D. M. Hien, and D. A. Lafontaine. 2020. Riboswitch regulation mechanisms: RNA, metabolites and regulatory proteins. *Biochim. Biophys. Acta. Gene Regul. Mech.* 1863:194501. <https://doi.org/10.1016/j.bbagr.2020.194501>.
- Lemay, J. F., G. Desnoyers, ..., D. A. Lafontaine. 2011. Comparative study between transcriptionally- and translationally-acting adenine riboswitches reveals key differences in riboswitch regulatory mechanisms. *PLoS Genet.* 7:e1001278. <https://doi.org/10.1371/journal.pgen.1001278>.
- Mandal, M., and R. R. Breaker. 2004. Gene regulation by riboswitches. *Nat. Rev. Mol. Cell Biol.* 5:451–463. <https://doi.org/10.1038/nrm1403>.
- Batey, R. T., S. D. Gilbert, and R. K. Montange. 2004. Structure of a natural guanine-responsive riboswitch complexed with the metabolite hypoxanthine. *Nature*. 432:411–415. <https://doi.org/10.1038/nature03037>.
- Mandal, M., M. Lee, ..., R. R. Breaker. 2004. A glycine-dependent riboswitch that uses cooperative binding to control gene expression. *Science*. 306:275–279. <https://doi.org/10.1126/science.1100829>.

32. Ren, A., K. R. Rajashankar, and D. J. Patel. 2012. Fluoride ion encapsulation by Mg^{2+} ions and phosphates in a fluoride riboswitch. *Nature*. 486:85–89. <https://doi.org/10.1038/nature11152>.
33. Montange, R. K., E. Mondragón, ..., R. T. Batey. 2010. Discrimination between closely related cellular metabolites by the SAM-i riboswitch. *J. Mol. Biol.* 396:761–772. <https://doi.org/10.1016/j.jmb.2009.12.007>.
34. Serganov, A., L. Huang, and D. J. Patel. 2008. Structural insights into amino acid binding and gene control by a lysine riboswitch. *Nature*. 455:1263–1267. <https://doi.org/10.1038/nature07326>.
35. Gilbert, S. D., F. E. Reyes, ..., R. T. Batey. 2009. Adaptive ligand binding by the purine riboswitch in the recognition of guanine and adenine analogs. *Structure*. 17:857–868. <https://doi.org/10.1016/j.str.2009.04.009>.
36. Serganov, A., and D. J. Patel. 2012. Molecular recognition and function of riboswitches. *Curr. Opin. Struct. Biol.* 22:279–286. <https://doi.org/10.1016/j.sbi.2012.04.005>.
37. Winkler, W. C., and R. R. Breaker. 2003. Genetic control by metabolite-binding riboswitches. *ChemBiochem*. 4:1024–1032. <https://doi.org/10.1002/cbic.200300685>.
38. Garst, A. D., A. L. Edwards, and R. T. Batey. 2011. Riboswitches: Structures and mechanisms. *Cold Spring Harbor Perspect. Biol.* 3:a003533. <https://doi.org/10.1101/cshperspect.a003533>.
39. Eskandari, S., O. Prychyna, ..., M. A. O'Neill. 2007. Ligand-directed dynamics of adenine riboswitch conformers. *J. Am. Chem. Soc.* 129:11308–11309. <https://doi.org/10.1021/ja073159l>.
40. Sudarsan, N., J. K. Wickiser, ..., R. R. Breaker. 2003. An mRNA structure in bacteria that controls gene expression by binding lysine. *Genes Dev.* 17:2688–2697. <https://doi.org/10.1101/gad.1140003>.
41. Sung, H.-L., and D. J. Nesbitt. 2020. Sequential folding of the nickel/cobalt riboswitch is facilitated by a conformational intermediate: Insights from single-molecule kinetics and thermodynamics. *J. Phys. Chem. B*. 124:7348–7360. <https://doi.org/10.1021/acs.jpcc.0c05625>.
42. Dambach, M., M. Sandoval, ..., G. Storz. 2015. The ubiquitous yybP-ykoY riboswitch is a manganese-responsive regulatory element. *Mol. Cell*. 57:1099–1109. <https://doi.org/10.1016/j.molcel.2015.01.035>.
43. Barrick, J. E., and R. R. Breaker. 2007. The distributions, mechanisms, and structures of metabolite-binding riboswitches. *Genome Biol.* 8:R239. <https://doi.org/10.1186/gb-2007-8-11-r239>.
44. Mellin, J. R., and P. Cossart. 2015. Unexpected versatility in bacterial riboswitches. *Trends Genet.* 31:150–156. <https://doi.org/10.1016/j.tig.2015.01.005>.
45. Hallberg, Z. F., Y. Su, ..., M. C. Hammond. 2017. Engineering and in vivo applications of riboswitches. *Annu. Rev. Biochem.* 86:515–539. <https://doi.org/10.1146/annurev-biochem-060815-014628>.
46. Blount, K. F., and R. R. Breaker. 2006. Riboswitches as antibacterial drug targets. *Nat. Biotechnol.* 24:1558–1564. <https://doi.org/10.1038/nbt1268>.
47. Hammes, G. G., Y.-C. Chang, and T. G. Oas. 2009. Conformational selection or induced fit: A flux description of reaction mechanism. *Proc. Natl. Acad. Sci. USA*. 106:13737–13741. <https://doi.org/10.1073/pnas.0907195106>.
48. Garst, A. D., A. Héroux, ..., R. T. Batey. 2008. Crystal structure of the lysine riboswitch regulatory mRNA element. *J. Biol. Chem.* 283:22347–22351. <https://doi.org/10.1074/jbc.C800120200>.
49. Blouin, S., R. Chinnappan, and D. A. Lafontaine. 2011. Folding of the lysine riboswitch: Importance of peripheral elements for transcriptional regulation. *Nucleic Acids Res.* 39:3373–3387. <https://doi.org/10.1093/nar/gkq1247>.
50. Earl, A. M., R. Losick, and R. Kolter. 2008. Ecology and genomics of *Bacillus subtilis*. *Trends Microbiol.* 16:269–275. <https://doi.org/10.1016/j.tim.2008.03.004>.
51. Huber, R., T. A. Langworthy, ..., K. O. Stetter. 1986. *Thermotoga maritima* sp. nov. represents a new genus of unique extremely thermophilic eubacteria growing up to 90°C. *Arch. Microbiol.* 144:324–333. <https://doi.org/10.1007/BF00409880>.
52. Gomes-Filho, J. V., and L. Randau. 2019. RNA stabilization in hyperthermophilic archaea. *Ann. N. Y. Acad. Sci.* 1447:88–96. <https://doi.org/10.1111/nyas.14060>.
53. Hu, E.-Z., X.-R. Lan, ..., D.-K. Niu. 2022. A positive correlation between GC content and growth temperature in prokaryotes. *BMC Genom.* 23:110. <https://doi.org/10.1186/s12864-022-08353-7>.
54. Hurst, L. D., and A. R. Merchant. 2001. High guanine-cytosine content is not an adaptation to high temperature: A comparative analysis amongst prokaryotes. *Proc. Biol. Sci.* 268:493–497. <https://doi.org/10.1098/rspb.2000.1397>.
55. Blouin, S., and D. A. Lafontaine. 2007. A loop loop interaction and a K-turn motif located in the lysine aptamer domain are important for the riboswitch gene regulation control. *RNA*. 13:1256–1267. <https://doi.org/10.1261/rna.560307>.
56. Fiegand, L. R., A. D. Garst, ..., D. J. Nesbitt. 2012. Single-molecule studies of the lysine riboswitch reveal effector-dependent conformational dynamics of the aptamer domain. *Biochemist.* 51:9223–9233. <https://doi.org/10.1021/bi3007753>.
57. Marton Menendez, A., and D. J. Nesbitt. 2022. Lysine-dependent entropy effects in the *B. subtilis* lysine riboswitch: Insights from single-molecule thermodynamic studies. *J. Phys. Chem. B*. 126:69–79. <https://doi.org/10.1021/acs.jpcc.1c07833>.
58. Szatmári, D., P. Sárkány, ..., M. Nyitrai. 2020. Intracellular ion concentrations and cation-dependent remodelling of bacterial MreB assemblies. *Sci. Rep.* 10:12002. <https://doi.org/10.1038/s41598-020-68960-w>.
59. Bennett, B. D., E. H. Kimball, ..., J. D. Rabinowitz. 2009. Absolute metabolite concentrations and implied enzyme active site occupancy in *Escherichia coli*. *Nat. Chem. Biol.* 5:593–599. <https://doi.org/10.1038/nchembio.186>.
60. Nicholson, D. A., A. Sengupta, and D. J. Nesbitt. 2020. Chirality-dependent amino acid modulation of RNA folding. *J. Phys. Chem. B*. 124:11561–11572. <https://doi.org/10.1021/acs.jpcc.0c07420>.
61. Dupuis, N. F., E. D. Holmstrom, and D. J. Nesbitt. 2013. Single-molecule kinetics reveal cation-promoted DNA duplex formation through ordering of single-stranded helices. *Biophys. J.* 105:756–766. <https://doi.org/10.1016/j.bpj.2013.05.061>.
62. Sung, H.-L., and D. J. Nesbitt. 2020. High pressure single-molecule FRET studies of the lysine riboswitch: Cationic and osmolytic effects on pressure induced denaturation. *Phys. Chem. Chem. Phys.* 22:15853–15866. <https://doi.org/10.1039/D0CP01921F>.
63. Sung, H.-L., and D. J. Nesbitt. 2022. Synergism in the molecular crowding of ligand-induced riboswitch folding: Kinetic/thermodynamic insights from single-molecule spectroscopy. *J. Phys. Chem. B*. 126:6419–6427. <https://doi.org/10.1021/acs.jpcc.2c03507>.
64. Dupuis, N. F., E. D. Holmstrom, and D. J. Nesbitt. 2018. Tests of Kramers' theory at the single-molecule level: Evidence for folding of an isolated RNA tertiary interaction at the viscous speed limit. *J. Phys. Chem. B*. 122:8796–8804. <https://doi.org/10.1021/acs.jpcc.8b04014>.
65. Fiore, J. L., E. D. Holmstrom, and D. J. Nesbitt. 2012. Entropic origin of Mg^{2+} -facilitated RNA folding. *Proc. Natl. Acad. Sci. USA*. 109:2902–2907. <https://doi.org/10.1073/pnas.1114859109>.
66. Kapanidis, A. N., T. A. Laurence, ..., S. Weiss. 2005. Alternating-laser excitation of single molecules. *Acc. Chem. Res.* 38:523–533. <https://doi.org/10.1021/ar0401348>.
67. Nicholson, D. A., B. Jia, and D. J. Nesbitt. 2021. Measuring excess heat capacities of deoxyribonucleic acid (DNA) folding at the single-molecule level. *J. Phys. Chem. B*. 125:9719–9726. <https://doi.org/10.1021/acs.jpcc.1c05555>.
68. Kinz-Thompson, C. D., N. A. Bailey, and R. L. Gonzalez, Jr. 2016. Precisely and accurately inferring single-molecule rate constants. *Methods Enzymol.* 581:187–225. <https://doi.org/10.1016/bs.mie.2016.08.021>.
69. Marton Menendez, A., and D. J. Nesbitt. 2023. Ionic cooperativity between lysine and potassium in the lysine riboswitch: Single-molecule kinetic and thermodynamic studies. *J. Phys. Chem. B*. 127:2430–2440. <https://doi.org/10.1021/acs.jpcc.3c00245>.

70. Garst, A. D., E. B. Porter, and R. T. Batey. 2012. Insights into the regulatory landscape of the lysine riboswitch. *J. Mol. Biol.* 423:17–33. <https://doi.org/10.1016/j.jmb.2012.06.038>.
71. Edwards, A. L., F. E. Reyes, ..., R. T. Batey. 2010. Structural basis for recognition of s-adenosylhomocysteine by riboswitches. *RNA*. 16:2144–2155. <https://doi.org/10.1261/rna.2341610>.
72. Holmstrom, E. D., and D. J. Nesbitt. 2016. Biophysical insights from temperature-dependent single-molecule Förster resonance energy transfer. *Annu. Rev. Phys. Chem.* 67:441–465. <https://doi.org/10.1146/annurev-physchem-040215-112544>.
73. Best, R. B., and G. Hummer. 2006. Diffusive model of protein folding dynamics with Kramers turnover in rate. *Phys. Rev. Lett.* 96:228104. <https://doi.org/10.1103/PhysRevLett.96.228104>.
74. Record, M. T., M. L. Lohman, and P. De Haseth. 1976. Ion effects on ligand-nucleic acid interactions. *J. Mol. Biol.* 107:145–158. [https://doi.org/10.1016/S0022-2836\(76\)80023-X](https://doi.org/10.1016/S0022-2836(76)80023-X).
75. Mikulecky, P. J., and A. L. Feig. 2006. Heat capacity changes associated with nucleic acid folding. *Biopolymers*. 82:38–58. <https://doi.org/10.1002/bip.20457>.
76. Ardehali, M. B., and J. T. Lis. 2009. Tracking rates of transcription and splicing in vivo. *Nat. Struct. Mol. Biol.* 16:1123–1124. <https://doi.org/10.1038/nsmb1109-1123>.
77. Sung, H. L., and D. J. Nesbitt. 2019. Novel heat-promoted folding dynamics of the yybP-ykoY manganese riboswitch: Kinetic and thermodynamic studies at the single-molecule level. *J. Phys. Chem. B*. 123:5412–5422. <https://doi.org/10.1021/acs.jpcc.9b02852>.
78. Lorenz, C., C. E. Lünse, and M. Mörl. 2017. tRNA modifications: Impact on structure and thermal adaptation. *Biomolecules*. 7:35–64. <https://doi.org/10.3390/biom7020035>.
79. Guo, F., and T. R. Cech. 2002. Evolution of tetrahymena ribozyme mutants with increased structural stability. *Nat. Struct. Biol.* 9:855–861. <https://doi.org/10.1038/nsb850>.
80. Disney, M. D., and D. H. Turner. 2002. Molecular recognition by the candida albicans group i intron: Tertiary interactions with an imino G·A pair facilitate binding of the 5' exon and lower the K_M for guanosine. *Biochemist.* 41:8113–8119. <https://doi.org/10.1021/bi020102x>.
81. Mathews, D. H., and D. H. Turner. 2002. Experimentally derived nearest-neighbor parameters for the stability of RNA three- and four-way multibranch loops. *Biochemist.* 41:869–880. <https://doi.org/10.1021/bi011441d>.
82. Znosko, B. M., M. E. Burkard, ..., D. H. Turner. 2002. Molecular recognition in purine-rich internal loops: Thermodynamic, structural, and dynamic consequences of purine for adenine substitutions in 5'(rGGCAAGCCU)₂. *Biochemist.* 41:14978–14987. <https://doi.org/10.1021/bi0203278>.
83. Leontis, N. B., and E. Westhof. 2001. Geometric nomenclature and classification of RNA base pairs. *RNA*. 7:499–512.
84. Lescoute, A., N. B. Leontis, ..., E. Westhof. 2005. Recurrent structural RNA motifs, isostericity matrices and sequence alignments. *Nucleic Acids Res.* 33:2395–2409. <https://doi.org/10.1093/nar/gki535>.